Using DEM-CFD method to predict Brownian particles deposition in a constricted tube

Florian Chaumeil[1], Martin Crapper[1]*
[1]*School of Engineering, the University of Edinburgh, Edinburgh EH9 3JL, United Kingdom*

Abstract

The modelling of the agglomeration and deposition on a constricted tube collector of colloidal size particles immersed in a liquid is investigated using the Discrete Element Method (DEM). The ability of this method to model surface interactions allows the modelling of particle agglomeration and deposition at the particle scale.The numerical model adopts a mechanistic approach to represent the forces involved in colloidal suspension by including near wall drag retardation, surface interaction and Brownian forces. The model is implemented using the commercially available DEM package EDEM 2.3®, so that results can be replicated in a standard and user-friendly framework. The effect of various particle-to-collector size ratios, inlet fluid flow-rates and particle concentrations are examined and it is found that deposition efficiency is strongly dependent on inter-relation of these parameters.

1 Introduction

Aggregation and deposition of particulate colloids (particle size between 1μm and 5μm diameter) on a solid surface is of great importance in many industrial processes such as micro-contamination control of microelectronics, membrane filtration, fouling of heat exchangers and surface deposition in micro-fluidic devices. In nature, micro-particle deposition is of great interest in microbial pathogen removal through natural granular filtration of surface water.

Deposition of inert colloids is also significant in water disinfection, since microbes and inert colloids exhibit important similarities in saturated porous granular media, as stated by Johnson et al (2007)[1], who observed that hydrodynamic drag mitigates deposition and drives re-entrainment of both biological and non-biological colloids.

As opposed to dissolved matter, which behaves as a continuum within the fluid medium, particulate matter is made of discrete entities that interact amongst themselves, with the fluid and with any physical boundaries. Modelling colloidal objects therefore requires specific numerical techniques that would allow the consideration of all these interactions. The Discrete Element Method (DEM) has been designed to model the flow of granular solids [2] by integrating the information (velocity, mass, collisions) of each individual particle. The present work uses DEM as framework enabling the consistent implementation of simulations of micro-scale particles and colloid dynamics therefore increasing reproducibility, visibility and impact.

This paper endeavours to define a model including relevant force models (interfacial interaction, retardation effect, Brownian effects) and numerical implementations that enable the simulation of hydraulically mediated colloidal surface interaction, flocculation and deposition by using the commercial DEM software EDEM 2.3® [3].

In order to model a solid-fluid system like particle-laden flow or suspensions, DEM computation can be coupled with Computational Fluid Dynamics (CFD). More generally, the DEM technique allows the consideration of the influence of external force fields by a using data map of the field. Independently, DEM also considers boundary-particle and particle-particle interactions, enabling the modelling of surface and interfacial forces. The force contribution of each interaction is added to the force balance and the equation of motion of each particle and then integrated [4].

Similarly the DEM approach has been successfully applied by Peng et al. [5] who developed a 2D in house DEM-based model to simulate nano-particle aggregation in a quiescent suspension influenced by an external alternating electrical field, over a broad pH range. Random Brownian diffusion and di-electrophoresis physics were implemented along with the standard DLVO forces. The present work represents an attempt to extend such a procedure to a 3D suspension flowing through constricted tubes. The deposition in a filter bed can be linked to the deposition in constricted tube through the approximate number of constricted tubes per unit area of filter.

Yoshida and Tien [6] experimentally studied the deposition of particles in a granular filter bed using sinusoidal constricted tubes. They plotted collection efficiency (that is the ratio between the amount of particles deposited and the number of particles injected) against the wall deposit concentration, in order to study re-entrainment, which was found to be a monotonic function of the extent of deposition. It was also stated that past a threshold wall concentration, a filter bed becomes non-retentive for particles equal to or less than 0.1μm. In the other hand, Marshall [7] reported the importance in the deposition process of particle-particle interaction (particle size exclusion combined with inter-particle DLVO interaction) by showing that aerosol channels with previously deposited particles and agglomerates had a higher capture rate of incoming particles. Bigger deposited agglomerates increase floc re-suspension [8]. Therefore particle-particle interactions in a flowing fluid are shown to be as critical as surface interaction. Results presented in the present paper will demonstrate that this conclusion is also true in hydrosols.

In order to simulate Brownian particle retention in the pore structure of a filter bed, Chang et al. [9] used a Brownian dynamics simulation of a constricted tube model. Particle diameter varied from 0.5 to 2 microns. They plotted the collection efficiency against the Reynolds number for different tube geometries. Like Johnson et al [1, 10, 11], they also encountered difficulty predicting deposition efficiency when wall and particle have similar surface charges (non favourable conditions) which demonstrates, the challenge faced when dealing with a secondary energy minimum. For this reason, in the first instance, the present paper will only consider favourable deposition conditions, where surface charges are not hindering deposition.

2 Definition of constricted tube geometry

The constricted tube geometry is used as a three-dimensional colloidal particle-tracking model that predicts colloid retention in porous media in favourable retention conditions (i.e. no electrostatic energy barrier). The geometry of the tube constriction and the inlet fluid conditions imposed define the flow field that is computed with CFD.

For comparison purposes, the constricted tube geometry used in this work corresponds to the parabolic constricted tube (PCT) described by Chang et al.[9, 12]

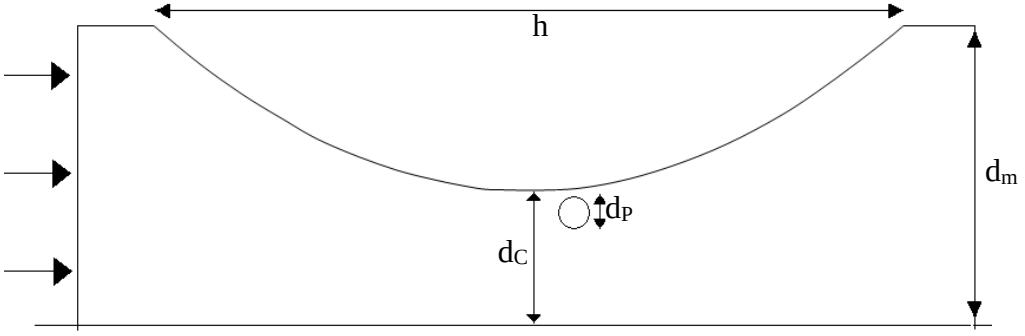

Figure 1: Parabolic Constricted Tube parameters definition

Universal constant	Value
h	100µm
d_P	1µm - 2µm
d_C	36µm
d_m	80µm

Table 1: geometrical parameters of the parabolic constricted tube

3 Numerical model

- Definition of the mechanistic model (forces)

Both the shape of the computational domain and the inlet condition (flow rate, inlet velocity distribution) define the flow field inside the tube. The trajectories of immersed particles within the flow field are integrated for different particle sizes, particle concentration and fluid flow rates following the method described below.

The Lagrangian method determines the trajectory of each particle under the effect of colloidal and external forces, and the governing equation of particle transport is the stochastic Langevin equation, including particle Brownian motion. Particle trajectory and particle deposition are controlled by the combined influence of colloidal and hydrodynamic interactions, this is described by the force balance equation (1) [11].

$$m\frac{du_p}{dt} = F_D + F_G + F_L + F_{EDL} + F_{LVdW} + F_B$$

Eq. 1

Where m is the particle mass and u_p is the particle velocity vector. F_D is the fluid drag, F_G the gravity, F_L the shear lift, F_{EDL} the electrostatic repulsion, F_{LVdW} the van der Waals attraction, and F_B the Brownian forces.

It is to be noted, however, that DEM is not commonly used to simulate processes involving very small finite particles, like colloids. The following paragraphs give an exhaustive list of the models and equations required to model the flow of a dilute colloidal suspension.

A. NEAR THE WALL HYDRAULIC RETARDATION

In the vicinity of a channel wall, the displacement of the fluid between the particle and the wall becomes increasingly difficult because of the fluid between the particle and the wall needing to be accelerated (see Figure 2).

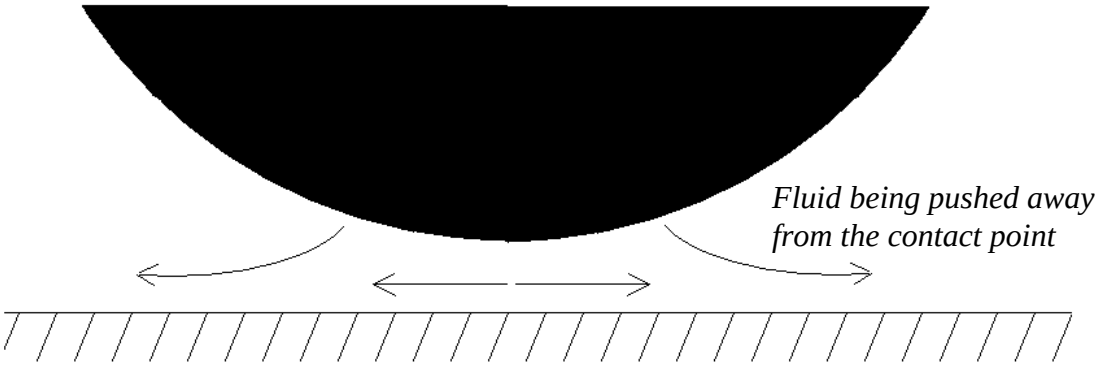

Figure 2: Fluid behaviour between a wall and an approaching particle [13]

This causes the particle to bear an additional hydrodynamic drag over the Stokes drag on the particle. Hence, near a channel wall, particle motion is retarded due to the presence of

the wall. Similarly, the presence of neighbouring particles causes the mutual retardation of the particles.

In order to consider this phenomenon let us express the 3D-vector of the particle velocity into the wall's local reference frame that is defined by the vector normal to the surface and two vectors normal to each other in the plane tangential to the surface.

Any motion of the particle relative to the wall can therefore be expressed as the sum of an velocity vector orthogonal to the wall with a velocity vector parallel to the wall. The following section explains how to use this decomposition to include the wall's presence effect.

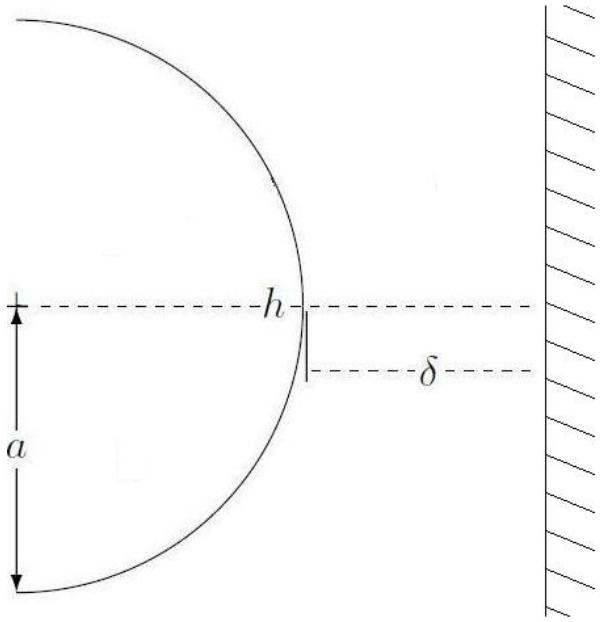

Figure 3: Fluid behaviour between a wall and an approaching particle

- Particle impinging Orthogonally on a rigid wall

The short-range hydrodynamic force, F, applied to a sphere with radius, R, can be described by the modified Stokes equation[11]:

$$F_{D\perp} = F_1 + F_2 = -6\pi\mu.aV.\lambda_{\perp} + 6\pi\mu.aU.f_2$$

Eq. 2

In equation 2, the drag is composed of the sum of two terms:

- First term, F_1, corresponds to the case where the particle with velocity V normal to the wall moves in a zero velocity field and therefore experiences a drag in the opposite direction of its velocity.
- the second term, F_2 corresponds to the case of a motionless particle within a liquid flow field with velocity U at the centre of the particle. The particle therefore experiences a drag in the same direction of the liquid velocity.

Equation 2 deviates from stokes law by the introduction of λ_t and f_2**,** correction factors that take into account the presence of a nearby wall. They are functions of the inter-surface separation distance, assuming a non-slip boundary condition applies to both the particle and solid surfaces. The factors tend to 1 at a large enough distance from the wall.

For the situation in which the sphere radius is small compared to the separation distance, Lorentz[14] found that the resistance of the particle is greater than would be predicted by Stokes' law by a factor $\lambda_{\perp}$. Independently of the ratio of radius to distance, Brenner [15](1961) calculated the general analytical expression for $\lambda_{\perp}$, the first two terms of the Taylor expansion of $\lambda_{\perp}$ being the Lorentz formula. Nguyen and Evans (2007) derived the exact and approximate expressions for resistance coefficients of a motionless colloidal sphere approaching a solid surface. In order not to hinder computation efficiency, analytical retardation functions are accurately approximated by simpler equations. For a solid particle approaching a much larger solid surface with non-slip boundary conditions at low Reynolds numbers, the approximate solution is [16]:

$$f_2 = \frac{2.022 + h/a}{0.626 + h/a}$$

And

$$\lambda_{\perp} = \left[1 + (a/h)^p\right]^{1/p}$$

With p=0.89

Eq. 3

- Translational and rotational motion of a sphere parallel to a rigid wall

Goldman et al (1967) [17, 18] developed asymptotic solutions for the near-wall hydrodynamic forces when a particle flows past an obstacle.

For a non-rotating sphere near a plane in a quiescent fluid, Goldman et al computed the asymptotic drag function:

$$F_{D//}^{t^*} \approx \frac{8}{15}\ln(\delta / a) - 0.9588$$

Eq. 4

Considering the linearity of Stokes equations, Goldman et al superimposed the force induced by a linear shearing flow past an immobilized sphere near a rigid wall:

$$F_{D//}^{s} = 6\pi\mu a Sh\left(1 + \frac{9}{16}\frac{a}{h}\right) \text{ with } U_f = sh\,.$$

Eq. 5

In the end the drag force acting on a sphere flowing closely along a wall is the sum of all contributions:

$$F_{D//} = 6\pi\mu a\left(UF_{D//}^{t^*} + a\Omega F_{D//}^{r^*} + Sh\left(1 + \frac{9}{16}\frac{a}{h}\right)\right)$$

Eq. 6

B. BROWNIAN MOTION AND DIFFUSION

For sub-micron sized particles, the local Stokes drag force must be corrected by a Cunningham factor [19], regardless of near the wall hydraulic retardation on the Stokes drag. The drag force expression is then given by:

$$F_D^{sub} = F_D^{ret} / C_C \text{ where } C_C = 1 + \frac{2\lambda}{d}\left(1.257 + 0.4e^{-0.55d/\lambda}\right)$$

Eq. 7

F_D^{ret} Is the usual drag force including the hydraulic retardation and λ is the molecular mean free path of the surrounding medium.

$$\lambda = \frac{\sqrt{mk_BT}}{\xi} \text{ [11]in a fluid and } \lambda = \frac{\mu}{\sqrt{2P\rho/\pi}} \text{ in a gas [20]}$$

Eq. 8

Where ξ is the drag or friction coefficient ($\xi = 6\pi.\mu.r_P$),k_B is the Boltzman constant and *T* is the temperature in Kelvin. Following the method used by Ounis et al. (1991) [19], the Brownian force components are independent white noise processes. At every time step, three independent Gaussian random numbers (G_i) of zero mean and unit variances are generated. These relate to the Brownian force (F_B), to be implemented in the momentum conservation equation (Eq. 1), by:

$$\overrightarrow{F_B} = \sum_{i=1}^{3} N_i \vec{e_i}$$

Eq. 9

Where N_i is the amplitude of the ith component of the Brownian force and has for expression:

$$N_i = G_i\sqrt{\frac{\pi S}{\Delta t}} \text{ where } S = \frac{2k_BTf}{\pi}; \quad f = \frac{6\pi\mu r_p}{C_c} \text{ so } N_i = G_i\sqrt{\frac{6\pi\mu r_p.2k_BT}{\Delta t.C_C}}$$

Eq. 10

C. DLVO FORCES

The interaction between two charged solute particles is generally expressed by the DLVO potential, which comprises an attractive Lifshitz–Van der Waals (LVdW) and a repulsive electrostatic double layer (EDL) interaction[21].

In this paper, we are restricting the simulation favourable condition, meaning only the Van-der-Waals force between two spherical surfaces immersed in a fluid medium is considered:

$$F_{lvdw} = \frac{32}{3}n^2\lambda\pi^2R\frac{b^3a^3}{\left(\left((R+a)^2-b^2\right)\left((R-a)^2-b^2\right)\right)^2}$$

Eq. 11

For two spheres of same radius and $h << a$

$$F_{lvdw} = \frac{Ha}{6h^2}$$

With $R = 2a + h$

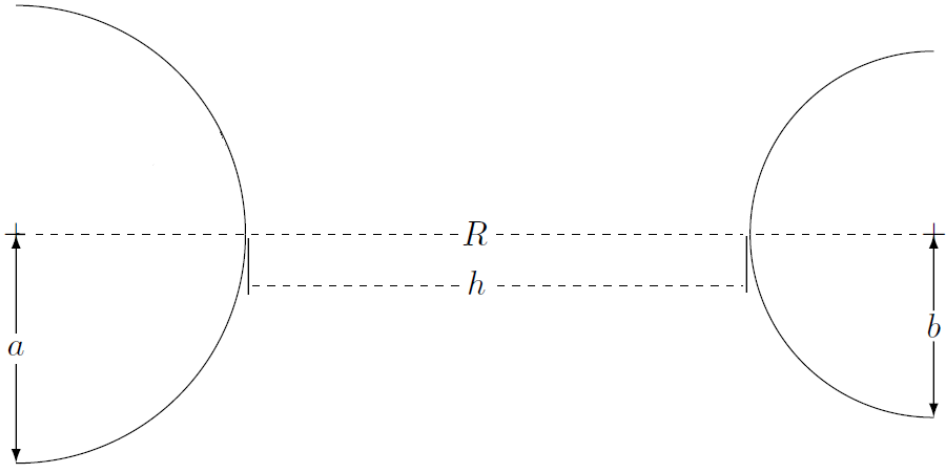

Figure 4: interaction between two spherical particles

Magnetic retardation effects should also be included as a multiplying factor in the Van der Waals force expression [22]:

$$f_m = \frac{\lambda(\lambda + 22.24h)}{(\lambda + 11.12h)^2}$$

Eq. 12

Table 2 summarises the forces influencing the dynamics of colloidal particle that need to be incorporated in the momentum conservation equation (Eq. 1).

Force	expression	Ref
Lipshitz-Van der Waals	$F_{lvdw} = \frac{32}{3} n^2 \lambda \pi^2 R \frac{b^3 a^3}{\left(\left((R+a)^2 - b^2\right)\left((R-a)^2 - b^2\right)\right)^2}$	[11, 21]
Drag	$F_{D\perp} = -6\pi\mu RV.\lambda_\perp + 6\pi\mu RU.f_2$ $F_{D//} = 6\pi\mu a\left(UF_{D//}^{t*} + a\Omega F_{D//}^{r*} + Sh\left(1 + \frac{9}{16}\frac{a}{h}\right)\right)$	[17, 18]
Brownian	$\overrightarrow{F_B} = \sum_{i=1}^{3} N_i \vec{e_i}$ with $N_i = G_i\sqrt{\frac{\pi S}{\Delta t}}$	[19]
Gravitational	$F_G = \frac{4}{3}\pi R^3\left(\rho_p - \rho_f\right)g$	
Shear Lift	$F_{SL} = 0.25.C.D_p^2.\rho_f\left(u_f - u_p\right)\sqrt{\nu\frac{\partial u_f}{\partial n}}$	[23]

Table 2: Expression of forces to be considered in the momentum conservation equation

4 Model implementation

- CFD method description

Although analytical solutions exist for flow fields inside constricted tube of regular geometries, this might not be the case for other system configurations, and therefore computational fluid dynamics (CFD) was used to derive the flow field. The commercial software Fluent 12.1 has been used to solve the steady-state Navier-Stokes equations under laminar flow hydrodynamics. The mesh was created to ensure residual convergence and stability. Because of the axi-symmetric nature of the constricted tube, simulations were carried out for only a tenth sector of the tube (Figure 3)

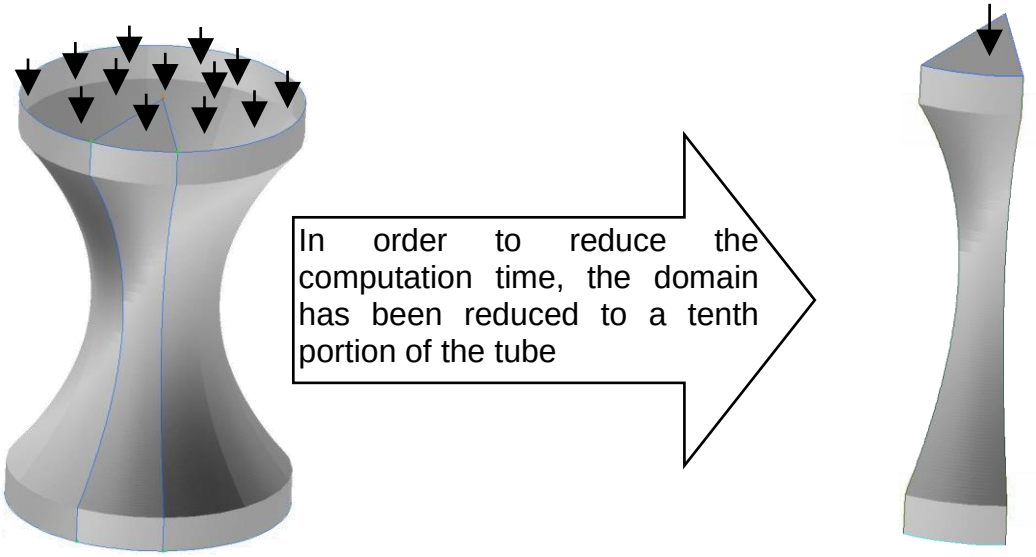

Figure 5: reduction of the computational domain

Boundary conditions for the model include no-slip boundaries at the tube wall surface, symmetry boundaries on both lateral boundaries of the slice and a predefined velocity inlet at the cell entry.

- DEM implementation description

Mechanistic principles are implemented via the EDEM™ 2.3 software which allows coupling with CFD data, with the ability, via API programming, to add the required force models.
Particles were created within an inlet control window of width y_0=5E-6µm (Figure 6), which stretches along the wall of the tube. Following the limiting trajectory model, particles injected further way from the wall would not contribute to the deposition process.

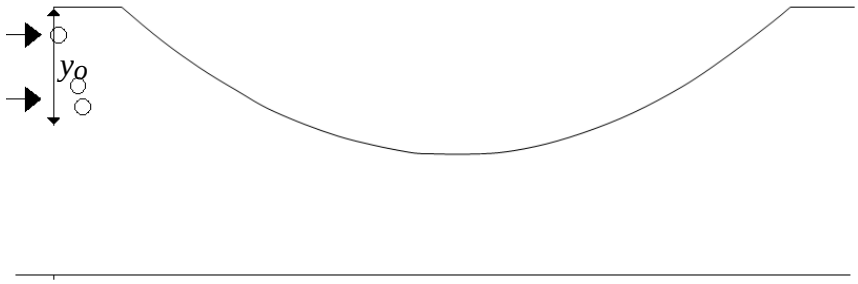

Figure 6: particle inlet window

Particles were randomly created one by one following a uniform law over the control window surface and the inlet particle concentration was tuned through the Particle creation rate Γ_{in} ranging from 5E3 $particles/s$ to 1E5 $particles/s$ this easily relates to the inlet bulk suspension's particle concentration [20] by:

$$C_0 = \frac{\Gamma_{in}}{A_w . V_{in}}$$

Eq. 13

For each single simulation, the computation was left running until the suspended particles escaped entirely and only the deposited particles remained in the computational domain. The collection efficiency could then be calculated as:

$$\eta = \frac{A_w}{A_{in}} . \frac{N_{dep}}{N_{gen}}$$

Eq. 14

Due to the high degree of randomness in the particle inlet, each simulation was repeated several times and the collection efficiency averaged over the range of the simulations.

- Limitations of the model

The current version of the EDEM software does not give the possibility to perform systematic analysis of the size distribution of the particle clusters as a function of either time or space. Such a feature would however be useful in order to support visual observations. Regarding the implementation of the particle mechanics immersed in water, the model described does not include hydraulic retardation between particles, which would be required for high particle concentrations. The implementation of surface interaction, surface roughness and heterogeneity has not been taken into account, although it was argued to have significant effect on particle deposition[24, 25].

5 Results and Discussion

The simulation parameters common to all tested configurations are presented in Table 3.

Universal constant	Value
Boltzmann constant k_B	1.381e-23 J/K
Temperature T	300 K
characteristic wave length λ	1e-7 m
Hamaker constant $H = n^2 \lambda \pi^2$	1.5e-20 J
Water dynamic viscosity μ	1e-3 kg.s/m
Density of particle ρ_P	1e3 kg/m^3

Table 3: simulation parameters

Specific configuration parameters are summed up in

Configurations	1: R1c5e3V001	2: R1c2e3V001	3: R1c1e4V002	4: R05c5e4V001	
particle radius (micron)	1	1	1	0.5	
velocity inlet (mm/s)	10	10	20	10	
inlet concentration (1/s)	5e3	2e3	1e4	5e4	
Collection efficiency (%)	1.42%	1.00%	0.31%	0.23%	with brownian motion
	3.09%				without Brownian motion

Table 4

Configurations	1: R1c5e3V001	2: R1c2e3V001	3: R1c1e4V002	4: R05c5e4V001	
particle radius (micron)	1	1	1	0.5	
velocity inlet (mm/s)	10	10	20	10	
inlet concentration (1/s)	5e3	2e3	1e4	5e4	
Collection efficiency (%)	1.42%	1.00%	0.31%	0.23%	with brownian motion
	3.09%				without Brownian motion

Table 4: configuration parameters and number of deposited particle for each configuration

The number of particles deposited in a parabolic constricted tube (PCT) obtained from the numerical model and simulation procedures described above with the purely attractive Van-der-Waals interaction energy curves are given in Figure 7, which clearly shows the

variability between different runs of same configuration, due both to the random particle generation and the randomness of cluster formation and re-suspension.

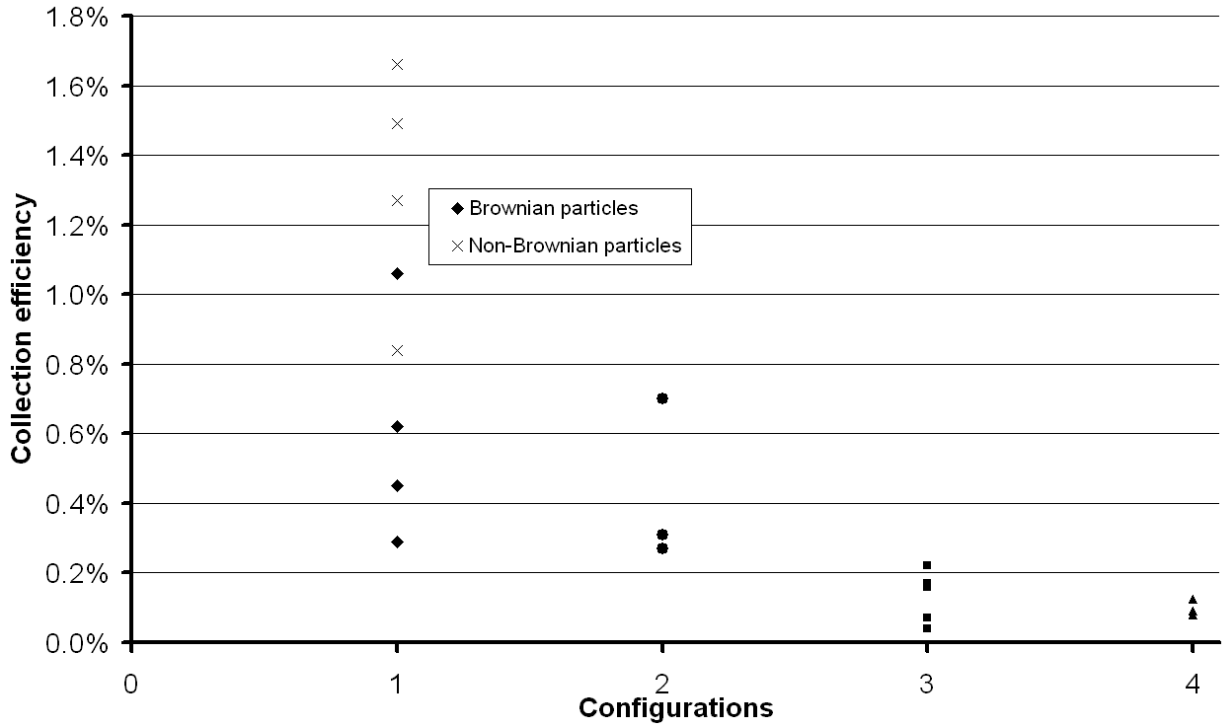

Figure 7: number of deposited particles for each configuration

- Effect of particle size on deposition

As a trend, for the range of particle sizes and concentration considered in this work, results show that the smaller the particle the less the chance of deposition. It is to be observed that for a given particle size, higher concentration induces higher deposition. The determining factor on particle deposition is not merely the size, but the ratio of total volume of particles flowing inside the tube with respect to the volume of the fluid domain. Interestingly, the total volume of particles is only the number of particles in the domain multiplied by the volume of each particle; so there is already a correlation to be observed between the size of particle and the concentration on the number deposited, the higher the volume of particle the higher the deposition. However, the number deposited does not increase linearly with the total volume of particles; this is due to impaction and scouring mechanisms as later described.

- Effect of suspension concentration and particle size exclusion

Fluid and particle material are chosen to have the same density, therefore inertial effects do not play any role in the particle deposition process. As they have a finite volume, the number of particle per unit of volume plays a critical role in aggregation. EDEM 2.3® allows considering the finite nature of particle volume, and results show that the major deposition mechanism identified is particle size exclusion, meaning that particles cannot physically overlap or occupy the same volume as another object. Instead, particles colliding then push each other, which is a major cause of lateral displacements and that induces wall aggregation.

- Particle deposition morphology

Flocculation behaviour of the particle suspension flowing through the tube is displayed on Figure **8**.

Both fluid and particles flow from the top of the figure to the bottom (though note that gravity was not included in the simulation and the orientation of the figure has no significance). In the region immediately downstream of the inlet, at the top of the figure, particles are evenly distributed due to the particles being injected following a uniform average distribution over the control window, corresponding to the particle inlet rate previously described. Particle inlet is in a smallregion near the wall, particles flowing at the centre being omitted, as following the limiting trajectory principle, they do not contribute to the deposition. Under the combined influence of the tube constriction, Brownian forces, particle volume and velocity gradient, the particles form clusters, or flocs, as they flow along the tube. Clusters grow while flowing through the constriction, and doing so, they segregate themselves from each other, meaning that distinct flowing aggregates are formed that are delimited by large, particle-free regions in between (see Figure **8**, configuration 1 and 3).

The deposition morphologies resulting from each configuration are displayed in Figure **9**. Along with Table 4 and Figure 7, it can be seen that collection efficiency decreases when concentration or particle size decreases, and also when flow rate increases.

The growth rate of the flocs increases with increasing particle concentration (as defined in Eq. 13) since particles are given more chance to collide through volume exclusion when a larger number of particles occupies the same volume. That, however, does not necessarily mean that particles deposit proportionally to the concentration: see columns 1 and 2 of Table 4, as flocs formation can have an adverse effect on deposition through impaction and scouring. This increases re-suspension via the mechanism shown in Figure **11** and described later. The re-suspension rate is defined as the ratio of deposited particles with respect to detached particles.

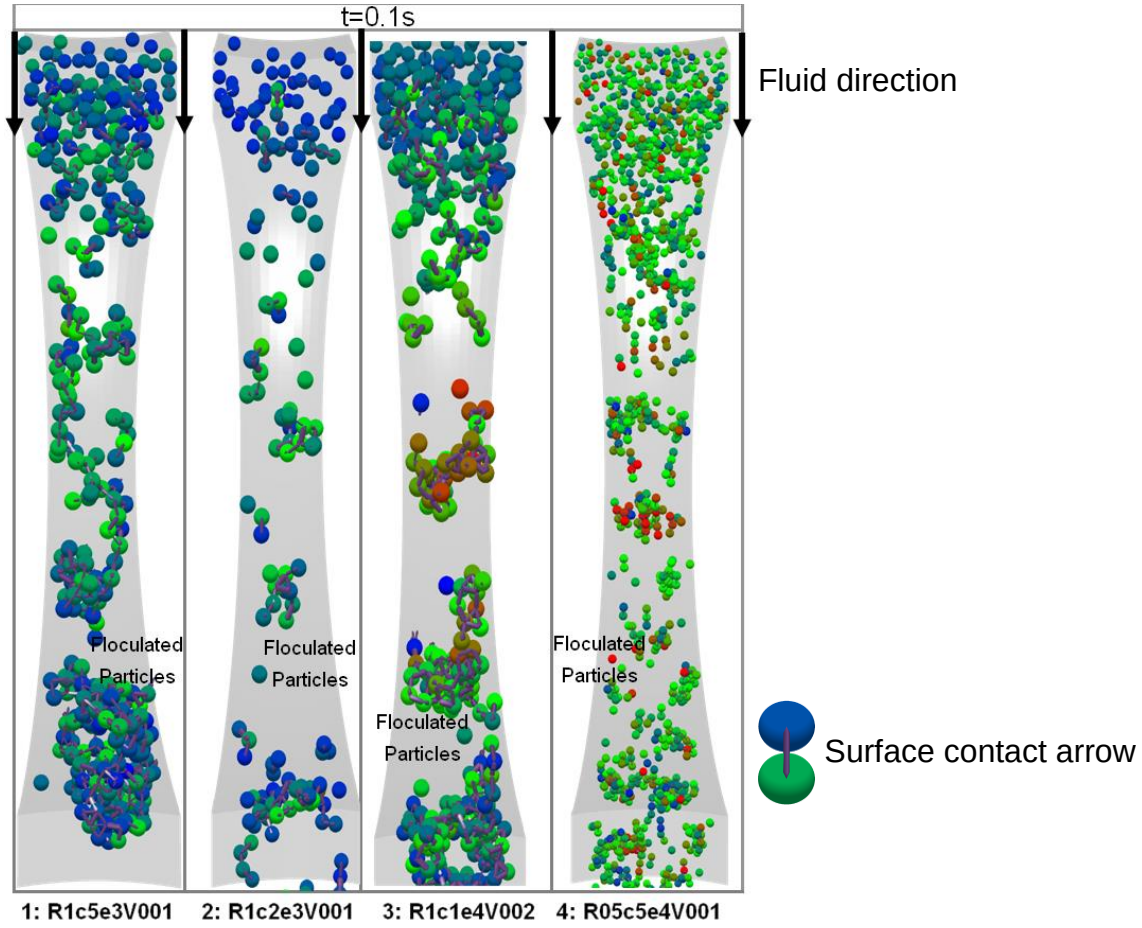

Figure 8: particle agglomeration during particle injection

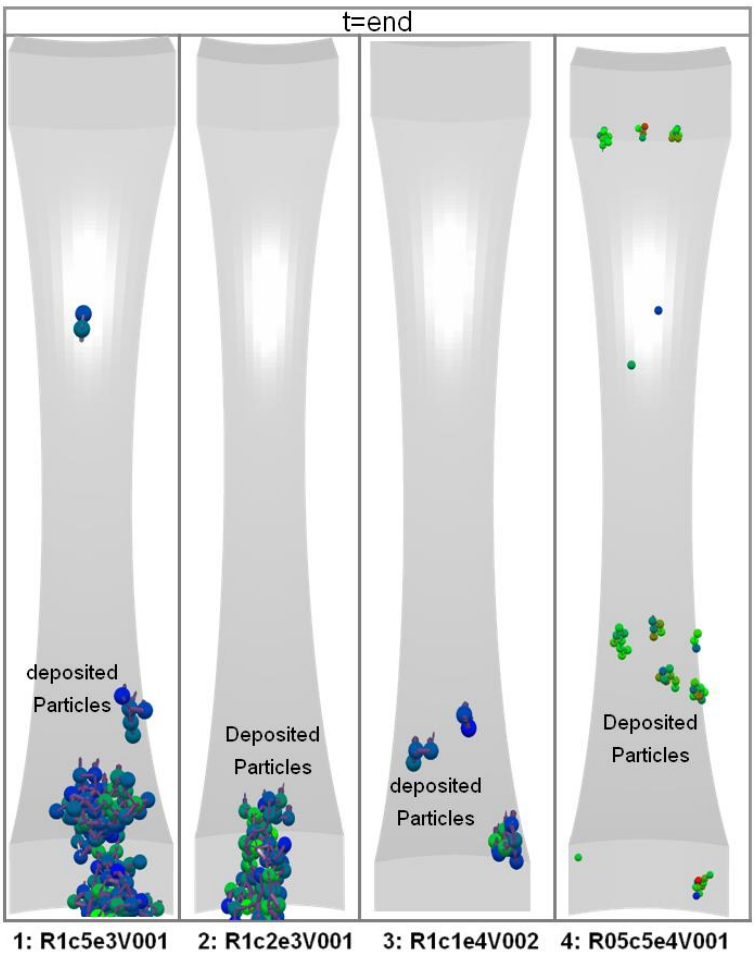

Figure 9: Deposited particles after free-flowing particles have escaped

- Effect of flow rate on deposition

The number of particles deposited where U_{in} = 0.1 cm/s is always greater than where Uin = 0.2 cm/s, hydraulic forces being much larger in the later case, so surface forces become less significant and re-suspension is easier.

Between configurations 1 and 3, the effect of flow rate on the size of flowing flocs can be compared visually. In order to keep the same volume concentration of particles, the particle creation rate was increased in the same proportion as the inlet velocity, following Eq. 13. Interestingly, from visual inspection the flow rate does not seem to influence the size of flowing clusters. Therefore, at given particle volume concentration, determining factors for cluster size can only be the remaining ones, meaning, the constriction geometry, the particle size and the other physical properties of the particles.

- Effect of Brownian motion

For configuration 1, a series of simulations have been performed with Brownian forces enabled and disabled. Results are displayed on Figure 7. As previously observed by Chang et al[12], Brownian particles have a lower collection efficiency than non-Brownian particles, which is explained by the random forces having an adverse effect on deposition, due to the Brownian forces being applied at each time step, uniformly in all directions i.e. mostly in directions non favourable to aggregation.

- Importance of cluster formation

Altmann [26] showed that deposited particles are either re-suspended as flocs or not at all, meaning that single deposited particles will not re-suspend due to hydrodynamic forces alone. Because of their bigger size, the side of deposited clusters closer to the centre of the tube is subjected to larger fluid forces than the cluster side near the wall.
Figure **10** plots the evolution of the number of deposited particles as a function of time;, by looking at the graphs one can clearly see the deposition and re-suspension behaviour.

If a cluster is loosely attached to the wall, i.e. via a small number of its particles, it can roll along the wall, attaching itself to the wall via different particles that successively attach and detach themselves from the wall as the cluster rolls. The rolling mechanism is generally associated on
Figure **10** with flattened peaks (indicated by the arrows). Where there are higher peaks, the clusters are bigger.

In some cases, the number of particles that attach the cluster to the wall is not enough to balance the fluid forces acting on the cluster, and it will re-suspend (
Figure **11**), meaning it is pulled back into the bulk of the suspension.

Aggregate or floc formation in the bulk of the fluid facilitates particle re-suspension by cluster collision and scouring; in fact, these phenomena are identifiable here as the main cause of particle detachment.
Figure **11** illustrates each step of the mechanism, where a deposited aggregate of particles (1), grows bigger by accumulating/catching free flowing particles and flocs, (2). Then either the impact (3) of the free flowing cluster will cause the initial deposited aggregate to re-suspend (4) or the newly agglomerated particle will cause the deposited aggregate to withstand higher hydraulic force without contributing to the cluster attachment to the wall, causing it to either roll or re-suspend directly.

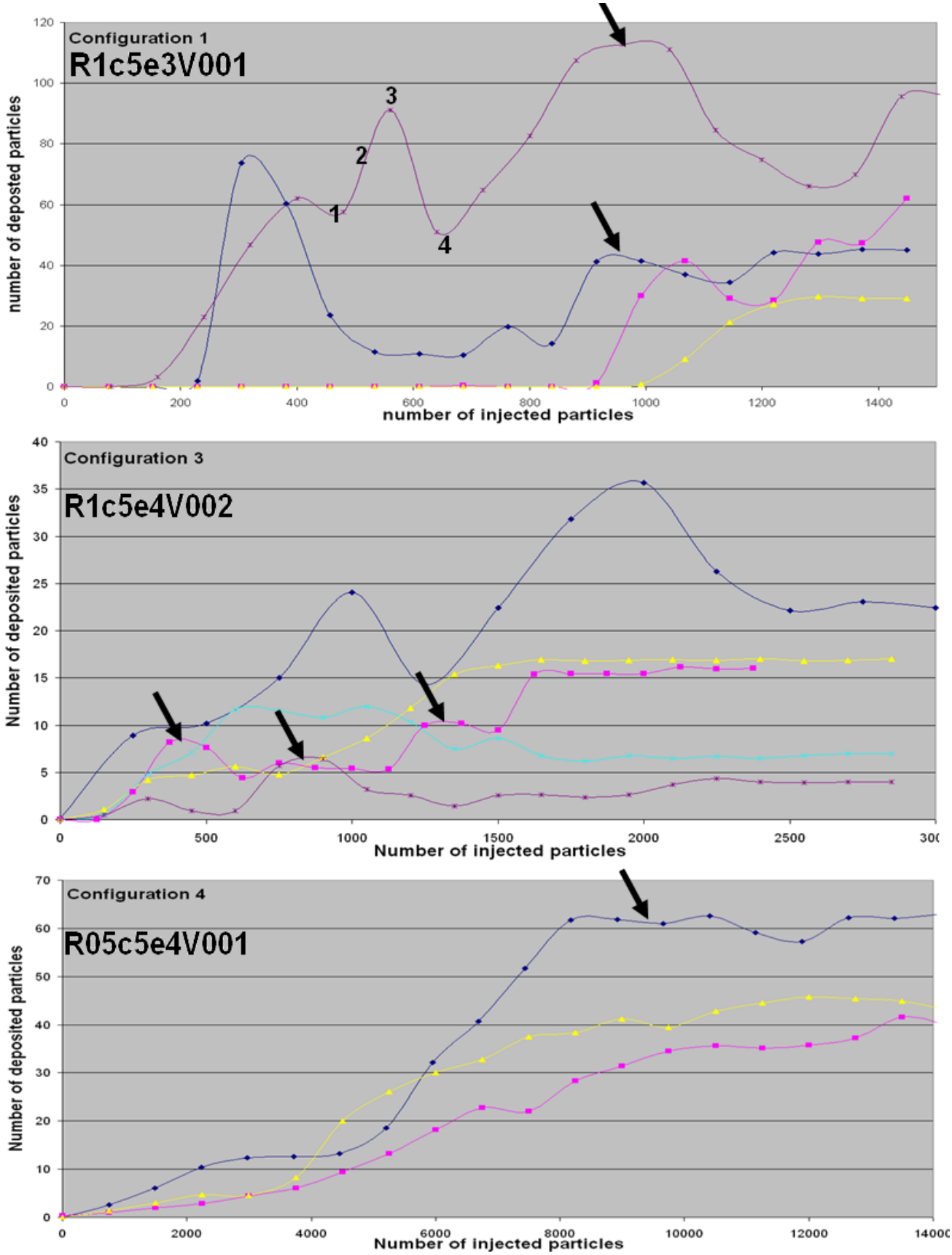

Figure 10: Evolution of particle deposition

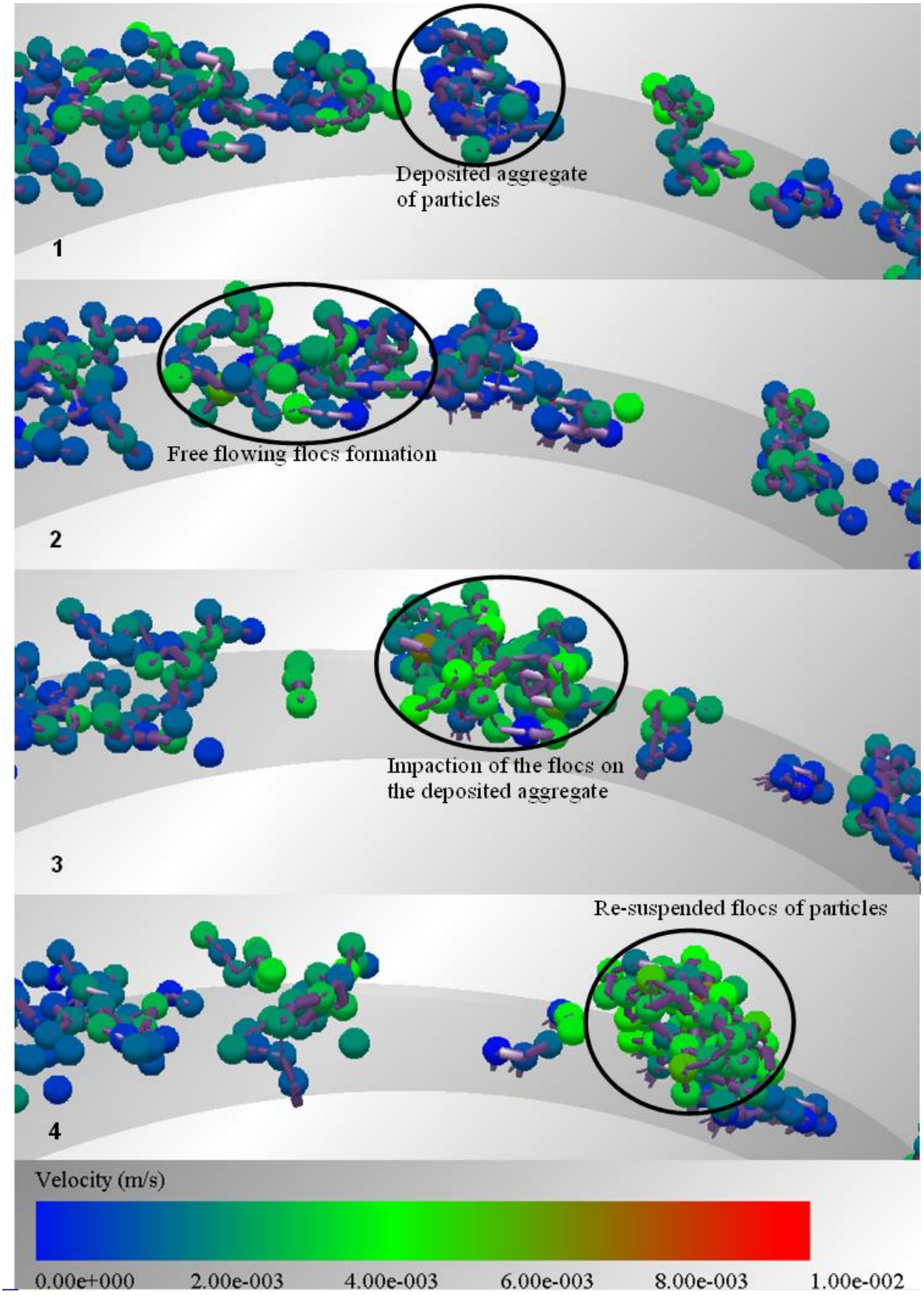

Figure 11: Frame by frame example of scouring mechanism on deposited particles

6 Conclusion

A series of particle scale simulations have been performed using DEM in order to numerically model flocculation and deposition of colloids in a constricted tube. Colloidal surface forces were implemented and interfacial Van der Waals interaction, retardation effects were considered along with Brownian forces. A numerical model was implemented through the commercial DEM software EDEM 2.3®, allowing the implementation of custom forces. A CFD computed velocity field was used to represent fluid velocity.

Results show that number of particles deposited does not increase linearly with the total volume of particles, but is controlled byimpact and scouring mechanisms. Graphs showing the evolution of the number of deposited particles in function of time can be interpreted to monitor the deposition and re-suspension behaviour of clusters of particle.

The ratio of total particle volume to fluid volume is a determining factor for deposition efficiency, due to the particles' lateral displacement resulting from volume exclusion and collision. Cluster formation influences deposition by increasing interception rate, which through impact, has an adverse effect on deposition. Collection efficiency is also reduced through cluster rolling and scouring.

Implementing colloidal forces with DEM-CFD technique through the commercial framework of EDEM2.3 has offered the ability to look easily into details of each of the particle deposition factors and their correlation between each other. DEM-CFD modelling in this context therefore represents an improvement on the previously published work, enables higher visibility and reproducibility, and broadens the number of possible users of such modelling.

References

1. Johnson, W.P., X. Li, and S. Assemi, *Deposition and re-entrainment dynamics of microbes and non-biological colloids during non-perturbed transport in porous media in the presence of an energy barrier to deposition.* Advances in Water Resources. **30**(6-7): p. 1432-1454.
2. Cleary, P.W. and M.L. Sawley, *DEM modelling of industrial granular flows: 3D case studies and the effect of particle shape on hopper discharge.* Applied Mathematical Modelling, 2002. **26**(2): p. 89-111.
3. DEMSolutionsLtd., www.dem-solutions.com.
4. Jing, L., O. Stephansson, and S. Lanru Jing and Ove, *Discrete Element Methods for Granular Materials*, in *Developments in Geotechnical Engineering*. 2007, Elsevier. p. 399-444.
5. Peng, Z., E. Doroodchi, and G. Evans, *DEM simulation of aggregation of suspended nanoparticles.* Powder Technology. **204**(1): p. 91-102.
6. Yoshida, H. and C. Tien, *Analysis of Brownian particle deposition and reentrainment in granular beds.* Journal of Colloid and Interface Science, 1986. **111**(1): p. 189-196.
7. Marshall, J.S., *Particle aggregation and capture by walls in a particulate aerosol channel flow.* Journal of Aerosol Science, 2007. **38**(3): p. 333-351.
8. Li, S.Q. and J.S. Marshall, *Discrete element simulation of micro-particle deposition on a cylindrical fiber in an array.* Journal of Aerosol Science, 2007. **38**(10): p. 1031-1046.

9. Chang, Y.I., S.C. Chen, and E. Lee, *Prediction of Brownian particle deposition in porous media using the constricted tube model.* Journal of Colloid and Interface Science, 2003. **266**(1): p. 48-59.
10. Johnson, W.P., E. Pazmino, and H. Ma, *Direct observations of colloid retention in granular media in the presence of energy barriers, and implications for inferred mechanisms from indirect observations.* Water Research. **44**(4): p. 1158-1169.
11. Ma, H., et al., *Hemispheres-in-Cell Geometry to Predict Colloid Deposition in Porous Media.* Environmental Science & Technology, 2009. **43**(22): p. 8573-8579.
12. Chang, Y.-I., et al., *A study on particle deposition morphology within a constricted tube in the presence and absence of the detachment mechanism.* Separation and Purification Technology, 2008. **63**(3): p. 566-576.
13. Pasol, L., et al., *Analytical solutions for a spherical particle near a wall in axisymmetrical polynomial creeping flows.* Physics of Fluids, 2005. **17**(7).
14. A., L.H., Abh. theoret. Phys, 1907. **1 23**.
15. Brenner, H., *The slow motion of a sphere through a viscous fluid towards a plane surface.* Chemical Engineering Science, 1961. **16**(3-4): p. 242-251.
16. Nguyen, A.V. and G.M. Evans, *Exact and approximate expressions for resistance coefficients of a colloidal sphere approaching a solid surface at intermediate Reynolds numbers.* Applied Mathematical Modelling, 2007. **31**(4): p. 763-769.
17. Goldman, A.J., R.G. Cox, and H. Brenner, *Slow viscous motion of a sphere parallel to a plane wall--I Motion through a quiescent fluid.* Chemical Engineering Science, 1967. **22**(4): p. 637-651.
18. Goldman, A.J., R.G. Cox, and H. Brenner, *Slow viscous motion of a sphere parallel to a plane wall--II Couette flow.* Chemical Engineering Science, 1967. **22**(4): p. 653-660.
19. Ounis, H., G. Ahmadi, and J.B. McLaughlin, *Brownian diffusion of submicrometer particles in the viscous sublayer.* Journal of Colloid and Interface Science, 1991. **143**(1): p. 266-277.
20. Tien, C. and B.V. Ramarao, *The process of particle deposition in granular media: Description and formulation*, in *Granular Filtration of Aerosols and Hydrosols (Second Edition)*. 2007, Butterworth-Heinemann: Oxford. p. 337-403.
21. Overbeek, E.J.W.V.a.J.T.G., *Theory of the Stability of Lyophobic Colloids.* 1948.
22. Gregory, J., *Approximate expressions for retarded van der waals interaction.* Journal of Colloid and Interface Science, 1981. **83**(1): p. 138-145.
23. Naumov, V.A., *Influence of Saffman's lift force on the motion of a particle in a Couette layer.* Journal of Engineering Physics and Thermophysics, 1995. **68**(5): p. 683-686.
24. Johnson, W.P., X. Li, and G. Yal, *Colloid Retention in Porous Media:â€‰ Mechanistic Confirmation of Wedging and Retention in Zones of Flow Stagnation.* Environmental Science & Technology, 2007. **41**(4): p. 1279-1287.
25. Bhattacharjee, S., C.H. Ko, and M. Elimelech, *DLVO interaction between rough surfaces.* Langmuir, 1998. **14**(12): p. 3365-3375.
26. Altmann, J. and S. Ripperger, *Particle deposition and layer formation at the crossflow microfiltration.* Journal of Membrane Science, 1997. **124**(1): p. 119-128.